Carbohydrate Polymers 95 (2013) 288–294

Contents lists available at SciVerse ScienceDirect

Carbohydrate Polymers

journal homepage: www.elsevier.com/locate/carbpol

Physicochemical studies of glucose, gellan gum, and hydroxypropyl cellulose—Inhibition of cast iron corrosion

Velayutham Rajeswari[a], Devarayan Kesavan[b], Mayakrishnan Gopiraman[b], Periasamy Viswanathamurthi[a,*]

[a] Department of Chemistry, Periyar University, Salem 636011, Tamil Nadu, India
[b] Department of Chemistry, National Institute of Technology, Tiruchirappalli 620015, Tamil Nadu, India

ARTICLE INFO

Article history:
Received 26 November 2012
Received in revised form 26 February 2013
Accepted 28 February 2013
Available online 7 March 2013

Keywords:
Carbohydrates
Cast iron
Adsorption
Langmuir
Synergism
Antagonism

ABSTRACT

Glucose, gellan gum, and hydroxypropyl cellulose were studied against the acid corrosion of cast iron by means of weight loss, potentiodynamic polarization, and AC impedance spectroscopy techniques. The inhibition efficiency was found to increase with increasing concentration of the inhibitors. The effect of immersion time and temperature were also studied. The addition of potassium iodide to the corrosion-inhibition system showed both antagonism and synergism toward inhibition efficiency. Polarization studies revealed the mixed-type inhibiting nature of the carbohydrates. The adsorption of inhibitors on the cast iron surface obeys Langmuir adsorption isotherm model, both in presence and absence of KI. Physical interaction between the inhibitor molecules and the iron surface was suggested by the thermochemical parameters, rather than chemical interaction.

1. Introduction

Cast iron is an indispensable material that is used to produce variety of objects found in day-to-day life due to its ductility, toughness and strength. Acid solutions are widely used in several industries for different purposes, for example, acid cleaning, acid pickling, descaling and oil wet cleaning and so on (Lagrenee, Mernari, Bouanis, Traisnel, & Bentiss, 2002; Li, Deng, Mu, Fu, & Yang, 2008). Metals and alloys, in general, tend to deteriorate under corrosive environments. The employment of inhibitors is one of the best-known methods to suppress the corrosion rate. The inhibitors containing electronegative functional groups such as sulphur, phosphorous, nitrogen, oxygen and aromatic rings have shown excellent corrosion retarding properties.

Polymers are one of the important types of corrosion inhibitors that have high affinity toward the metal surfaces (Kesavan, Gopiraman, & Sulochana, 2012). Carbohydrates are the most abundant renewable materials in natural resources. The derivatives of carbohydrates are very useful biomaterials for several applications (Klemm, Schmauder, & Heinze, 2002). However, very few natural and semi-synthetic carbohydrates were studied for the subject of corrosion inhibition. For example, carboxymethyl cellulose (Bayol, Gürten, Dursun, & Kayakirilmaz, 2008; Solomon, Umoren, Udosoro, & Udoh, 2010; Umoren, Solomon, Udosoro, & Udoh, 2010), guar gum (Abdallah, 2004), Arabic gum (Umoren, Ogbobe, Igwe, & Ebenso, 2008), and starch (Bello et al., 2010; Mobin, Khan, & Parveen, 2011) were examined for corrosion inhibition of steels in different acid medium. Exudate gum (Umoren, Obotl, Ebenso, & Okafor, 2008) was also reported as a corrosion inhibitor for aluminum in an acid medium.

In view of material properties, inexpensiveness, and potential environmental benefits, in this study, gellan gum and hydroxypropyl cellulose were evaluated against the acid corrosion of cast iron. It is much interesting to compare the efficacy of a monosaccharide with polysaccharides. Therefore, glucose was also examined for corrosion inhibition. The inhibitors were evaluated by means of weight loss, potentiodynamic polarization, and electrochemical impedance spectroscopy (EIS) techniques. The addition of halide ions alongside with inhibitors increases the inhibition potential of the inhibitor with decreasing the amount of the inhibitor required. Therefore, the effect of KI addition to the corrosion-inhibition system was also studied. In order to understand the adsorption mechanism of the inhibitors, the inhibitors adsorbed on the steel surface were analyzed by Fourier transform infrared spectroscopy (FT-IR), wide-angle X-ray diffraction (WAXD) and the morphological changes on the iron specimens were observed under scanning electron microscopy (SEM) and the results were presented in the following sections.

* Corresponding author. Tel.: +91 427 2345271; fax: +91 427 2345124.
E-mail address: viswanathamurthi72@gmail.com (P. Viswanathamurthi).

0144-8617/$ – see front matter © 2013 Elsevier Ltd. All rights reserved.
http://dx.doi.org/10.1016/j.carbpol.2013.02.069

2. Experimental

2.1. Materials and methods

Corrosion tests were performed using cast iron consisting of the following composition (wt%) C, 6.09; Al, 1.13; Mn, 0.78 and the remainder being Fe. The cast iron specimens were cut into dimensions of 1 cm × 1 cm × 0.02 cm and the surface was abraded with a series of emery papers from grades 600, 800, 1000, and 1200. The specimens were washed with double distilled water, degreased with acetone and then dried at room temperature. The electrolyte solution, 1 M HCl, was prepared from analytical grade HCl (Merck) using double distilled water. The inhibitor glucose (**A**) was purchased from lobo chemie, whereas, gellan gum (**B**) and hydroxypropyl cellulose (**C**) were purchased from Sigma Aldrich. The chemical structures of the inhibitors were shown in the Fig. S1 (see supporting information). The inhibitor solutions at concentrations 100, 200, 300, 400, and 500 ppm were prepared in 1 M HCl solution. Potassium iodide (KI) was supplied by Merck and the aqueous solutions were prepared at concentrations 1, 3, 5, 7, 9 and 11 ppm.

2.2. Weight loss measurements

Weight loss experiments were carried out similar to the procedure described in the earlier reports (Gopiraman, Selvakumaran, Kesavan, & Karvembu, 2012; Kesavan, Muthu Tamizh, Gopiraman, Sulochana, & Karvembu, 2012; Rajeswari, Kesavan, Gopiraman, & Viswanathamurthi, 2013). In brief, cast iron specimens in triplicate were immersed in 100 mL of 1 M HCl solution containing different concentrations of the studied inhibitors for 2 h at different temperatures (298, 308, 318, and 328 ± 1 K). Specimens were weighed before and after immersion, and the weight differences were determined. Average values of three experiments were used for calculations.

The surface coverage (θ) and percentage inhibition efficiency (IE%) were calculated by using the following equations:

$$\text{Surface coverage} = \frac{W_0 - W}{W_0} \quad (1)$$

$$\text{IE\%} = \text{surface coverage} \times 100 \quad (2)$$

where W_0 and W are the weight losses of iron specimen observed in the absence and presence of each inhibitor, respectively. In order to study the effect of halide additives, along with the inhibitor, small quantity of KI (in ppm) were applied to the corrosive media.

2.3. Electrochemical measurements

The electrochemical measurements were performed using a CHI 760C electrochemical analyzer. A traditional three-electrode system that consists of a platinum electrode, saturated calomel electrode, and the iron specimen were used as the counter electrode, reference electrode, and working electrode, respectively. The working electrode was a cast iron specimen having an exposed area of 1 cm^2 and the rest being coated with a resin. Prior to each measurement, the working electrode was polished with emery papers, washed with double distilled water and acetone.

The working electrode was immersed into the test solution for 30 min to reach a steady state open circuit potential. The Tafel polarization curves were obtained at a potential range from −0.2 to −0.8 V *versus* open circuit potential with a scan rate of 0.01 V/s. A detailed experimental procedure was described in our previous report (Rajeswari et al., 2013). The inhibition efficiency IE% was calculated by following Eq. (3):

$$\text{IE\%} = \frac{I'_{corr} - I_{corr}}{I'_{corr}} \times 100 \quad (3)$$

where I'_{corr} and I_{corr} are uninhibited and inhibited corrosion current densities, respectively.

The electrochemical impedance spectroscopic (EIS) experiments were conducted at open circuit potential in the frequency range of 10^4–10^1 Hz and the amplitude was 0.005 V. All the impedance values were measured at the open circuit potential and were analyzed in terms of the equivalent circuit shown in supporting information (Fig. S2, see supporting information). In the given electrical equivalent circuit, R_s is the solution resistance, R_{ct} is the charge transfer resistance, and C_{dl} is the double layer capacitance. Nyquist plots were made from these experiments. Double layer capacitance (C_{dl}) and IE% were calculated from the following equations:

$$C_{dl} = \frac{1}{2\pi \times f_{max} \times R_{ct}} \times 100 \quad (4)$$

$$\text{IE\%} = \frac{R'_{ct} - R_{ct}}{R'_{ct}} \times 100 \quad (5)$$

where f_{max} is the frequency at apex on the Nyquist plot, R'_{ct} and R_{ct} are the charge transfer resistance values of inhibited and uninhibited solutions, respectively. All EIS measurements were carried out at 298 ± 1 K.

2.4. FT-IR spectroscopy

The cast iron specimens were immersed in 1 M HCl solution containing optimum concentration (500 ppm) of inhibitors (**A**–**C**). After 2 h of immersion, the specimens were removed, rinsed quickly with acetone and dried at room temperature. The inhibitor adsorbed on the cast iron surface was scraped carefully using a knife and the scraped samples were designated as Inh_{ads}, which were subjected to FT-IR spectroscopy (a PerkinElmer FT-IR spectrometer).

2.5. Wide angle X-ray diffraction

X-ray diffraction analysis of the inhibitors **A**–**C**, and the Inh_{ads} was examined by using a Rotaflex RTP300 X-ray diffractometer (Rigaku Co., Japan). X-ray diffractometer was controlled at 50 kV and 200 mA. Nickel filtered Cu Kα radiation was used for the measurements with an angular range of $5^\circ < 2\theta < 70^\circ$ at room temperature.

2.6. Scanning electron microscopy

The cast iron specimens were immersed in blank (1 M HCl) solution and solutions having optimum inhibitors concentration (500 ppm of **A**, **B**, and **C**) for 2 h. The specimens were washed with distilled water and acetone and then instantaneously observed under SEM (a Hitachi model-3000H) to examine the surface morphological change.

3. Results and discussion

3.1. Weight loss measurements

3.1.1. Effect of inhibitor concentration

The values of IE%, surface coverage (θ), and standard deviation (σ) were given in Table 1. The IE% was found to increase along with the increment of the inhibitors' concentration by suppressing the corrosion rate. The inhibitors **A**, **B**, and **C** showed IE% of 70%, 81%,

Table 1
Weight loss, inhibition efficiency and surface coverage for different concentrations of inhibitors for the corrosion of cast iron in 1 M HCl from weight loss measurements at 298 ± 1 K.

Inhibitor	Concentration of inhibitor (ppm)	Weight loss (g/h)	IE%[a]	θ[b]	σ[c]
(Blank)	0	0.0184	–	–	–
A	200	0.0105	42.9	0.43	0.03
	300	0.0092	50.1	0.50	0.01
	400	0.0075	59.2	0.59	0.07
	500	0.0056	69.5	0.70	0.11
B	200	0.0064	65.2	0.65	0.05
	300	0.0058	68.4	0.68	0.03
	400	0.0048	73.9	0.74	0.05
	500	0.0035	80.9	0.81	0.02
C	200	0.0046	75.0	0.75	0.02
	300	0.0037	79.8	0.80	0.01
	400	0.0027	85.3	0.85	0.09
	500	0.0019	89.6	0.90	0.03

[a] IE% – percentage inhibition efficiency.
[b] θ – surface coverage.
[c] σ– standard deviation for IE%.

and 90% respectively. Among the studied inhibitors, hydroxypropyl cellulose (**C**) exhibited higher IE%, which is attributed to its molecular structure. The propylene oxide units in the side chain of **C** may extend its interaction with the metal surface better than inhibitors **A** and **B**. The polymeric structure of the inhibitors **B** and **C**, which have more sites for interaction with the metal surface, resulted in higher IE% than inhibitor **A**, a monosaccharide. In the cases of **A** and **C**, further increase of concentrations more than 500 ppm did not give any significant increase in IE%. For inhibitor **B**, phase separation was found in solutions having concentrations more than 500 ppm.

3.1.2. Effect of temperature

For inhibitors **A** and **C**, the IE% decreases when the temperature was raised (see Table S1 in supporting information), which suggests that these inhibitors adsorb through weak physical interactions that disappear at elevated temperatures. Meanwhile, inhibitor **B** showed a gradual increase in IE% upto 85% at 328 K, which was higher than its corresponding IE% (81%) at 298 K. The results implied that the inhibitor **B** might act via chemical adsorption at elevated temperatures to retard the corrosion rate (Ammar & Khorafi, 1973). This phenomenon was attributed to the presence of carboxyl group in **B**, which is classified in spectrochemical series as a better ligand than the hydroxyl groups (Huheey, Keiter, Keiter, & Medhi, 1993).

3.1.3. Adsorption isotherm and thermochemical parameters

In order to recognize the mechanism of corrosion inhibition, the values of surface coverage (θ) corresponding to different concentrations of inhibitors **A**–**C** in the temperature range from 298 to 328 K. They were tested by fitting different adsorption isotherms such as Langmuir, Temkin, Frumkin and Freundlich adsorption isotherms. Based on the correlation coefficient values (Table 2), Langmuir adsorption isotherm (Eq. (6), and see Fig. S3 in supporting information) was found to fit the experimental values obtained from weight loss measurements.

$$\frac{C_{\text{inh}}}{\theta} = \frac{1}{K_{\text{ads}}} + C_{\text{inh}} \tag{6}$$

where θ is the surface coverage, C_{inh} is the concentration of inhibitors and K_{ads} is the equilibrium constant for the adsorption process. Though the weight loss data were found to fit the Langmuir adsorption isotherm, the ideal nature of the slope, *i.e.* unity, was not achieved. In the case of Temkin and Frumkin isotherms no significant correlations were observed, as the R^2 values were less than 0.99 (see supporting information, Table S2, Figs. S4 and S5). The correlation coefficient value for Freundlich isotherm (Fig. S6 in supporting information) of inhibitor **A** was 0.993, suggested the involvement of both physical and chemical factors in the adsorption process (Yang, 1998).

Similar observations were reported for many organic inhibitors including carboxymethyl cellulose (Solomon et al., 2010; Umoren et al., 2010). A possible explanation for the deviation of slope from 1.0 can be the interaction between the inhibitor molecules that were adsorbed on the metal surface (Ammar, Darwish, & Etman, 1967).

The thermochemical parameters (given in Eqs. (7)–(9)) such as K_{ads}, ΔG_{ads}, ΔS_{ads}, and ΔH_{ads} were calculated similar to our previous report (Kesavan, Muthu tamizh, et al., 2012; Rajeswari et al., 2013) and the data were presented in Table 2. For inhibitors **A** and **C**, the K_{ads} values decreased with rising temperature, which indicated that these inhibitors might have physically adsorbed on the metal surface. Meanwhile, **B** showed increase of K_{ads} at elevated temperatures, which suggested for possible chemical adsorption of inhibitor molecules on the metal surface. The negative values of ΔG_{ads} ensure the spontaneity of adsorption process and stability of the adsorbed layer on the surface. The dependence of ΔG_{ads} on temperature can be explained by two cases as follows: (a) ΔG_{ads} may increase (becomes less negative) with the increase of temperature, which shows the occurrence of exothermic process. (b) ΔG_{ads} may decrease (becomes more negative) with increasing temperature signifying the occurrence of endothermic process. Generally, the magnitude of ΔG_{ads} around −20 kJ/mol or less negative is assumed for electrostatic interactions that exist between inhibitor and the charged metal surface (*i.e.* physisorption). While those around −40 kJ/mol or more negative are indicating charge sharing or transferring from organic species to the metal surface to form a coordinate type of metal bond (*i.e.* chemisorptions) (Noor, 2007).

$$\Delta G_{\text{ads}} = -RT\ \ln(55.5K_{\text{ads}}) \tag{7}$$

$$\text{Intercept} = \log\ \left(\frac{R}{Nh}\right) + \frac{\Delta S_{\text{ads}}}{2.303R} \tag{8}$$

$$\Delta H_{\text{ads}} = \Delta G_{\text{ads}} + T\Delta S_{\text{ads}} \tag{9}$$

where R is the gas constant (8.314 J K^{-1} mol^{-1}), T is the absolute temperature, 55.5 is the concentration of water in solution, K_{ads} is the equilibrium constant, ΔG_{ads} is free energy of adsorption, N is Avagadro's number, h is planck's constant, ΔH_{ads} is standard enthalpy of adsorption, ΔS_{ads} is standard entropy of adsorption.

Table 2
Thermodynamic parameters for cast iron in 1 M HCl in the presence of inhibitors (500 ppm) at different temperatures.

Inhibitor	Temperature (K)	R^2	K_{ads} (kJ/mol)	ΔG_{ads} (kJ/mol)	ΔS_{ads} (J K^{-1} mol^{-1})	ΔH_{ads} (kJ/mol)
A	298	0.992	21.57	−23.79	−95.50	28.48
	308	0.996	16.97	−25.11	–	–
	318	0.996	11.14	−26.70	–	–
	328	0.995	10.94	−27.65	–	–
B	298	0.992	54.84	−20.52	−105.3	31.39
	308	0.992	58.55	−20.76	–	–
	318	0.983	61.39	−21.10	–	–
	328	0.981	68.03	−21.00	–	–
C	298	0.997	65.97	−19.71	−127.7	38.07
	308	0.983	64.05	−20.27	–	–
	318	0.981	62.37	−21.02	–	–
	328	0.996	56.90	−22.06	–	–

In the present study, the ΔG_{ads} values of the inhibitors **A**–**C** were ranging from −20.3 kJ/mol to −27.6 kJ/mol indicating that the studied inhibitors act predominantly *via* physisorption. The value of ΔS_{ads} was attributed to the occurrence of a substitution process (given in Eq. (10)) for the period of inhibitor adsorption on the metal surface. The negative sign of the entropy implies that the activated complex in the rate determining step represents association rather than dissociation step. The positive signs of the enthalpies reflect the endothermic nature of the steel dissolution process and means that the dissolution of steel is difficult (Behpour et al., 2008).

$$m\,H_2O_{(surface)} + n\,Inhibitor_{(solution)} \rightarrow x\,Inhibitor_{(surface)} + y\,H_2O_{(solution)} + (n-x)\,Inhibitor_{(solution)} + (m-y)\,H_2O_{(surface)} \quad (10)$$

where m and n are the number of water and inhibitor molecules present on the surface and in the solution, respectively. y number of water molecules from the surface were replaced by x number of inhibitor molecules from the bulk. Therefore the number of inhibitor molecules available in the bulk is $n-x$ and the number of water molecules available on the surface is $m-y$. This representation is ideally suitable for representing the interaction between inhibitor molecules and the iron surface, where the effect of chloride ions is ignored.

3.1.4. Effect of KI

The results of addition of KI to the corrosion-inhibition system were given in Table S3. Initially, at lower concentrations of KI, the IE% were lesser than the corresponding values at 298 K for all the inhibitors, which indicated the antagonistic behavior of KI + inhibitor on IE%. Upon increasing the concentration of the KI showed a gradual increase in the IE% values. The inhibitor **A** showed a maximum IE% of 74.2%, while **B** and **C** exhibited 94.1% and 96.9%, respectively at 11 ppm of KI. The synergistic effect between inhibitors and iodide (I^-) ions can be explained by the fact that the addition of the KI constituent stabilized the adsorption of inhibitors on cast iron. Further increment in concentration of KI did not give any significant rise of IE%.

Naturally, halides have tendencies to both inhibit and increase the corrosion of metals at given circumstances. A detailed experiment for the effect of I^-, Br^-, and Cl^- on the inhibitive characteristics of carboxymethyl cellulose (CMC) was reported by Umoren et al. (2010). Similar to the present studies, for CMC antagonism followed by synergism was observed upon addition of halides. The antagonistic nature of CMC + halides was attributed to the formation of soluble intermediates during adsorption process.

3.2. Polarization measurements

Potentiodynamic anodic and cathodic polarization plots for cast iron specimens in 1 M HCl solution in the absence and presence of different concentrations of inhibitors were shown in Fig. 1. The electrochemical kinetic parameters such as corrosion current density (I_{corr}), corrosion potential (E_{corr}), cathodic slope (b_c), and anodic slope (b_a) were calculated and given in Table 3. The results indicated that the current density decreases with increasing the inhibitors concentration. Though, the suppression of both anodic and cathodic reactions was observed, the inhibitors predominantly retarded anodic reaction. This result suggests that the addition of the inhibitors decreases anodic dissolution and also slow down the hydrogen evolution reaction. No definite trend was observed in the shift of E_{corr} values in the presence of different concentrations of the inhibitors, signifying that these inhibitors behave as mixed-type inhibitors.

3.3. Electrochemical impedance spectroscopy (EIS)

The Nyquist plot obtained from EIS measurements and the results were given in Fig. 2 and Table 4. It is clear from these plots that the impedance response of cast iron in uninhibited 1 M HCl has considerably changed after the addition of inhibitors into the corrosive solutions. Nyquist plots size increased with the inhibitor concentration suggested that the produced inhibitive film was strengthened by addition of inhibitors and also charge transfer process mainly controlling the corrosion of cast iron. The charge-transfer resistance (R_{ct}) values were calculated from the difference in impedance at lower and higher frequencies. The R_{ct} values increased and the values of C_{dl} decreased with an increase in the inhibitors concentration which is attributed to the rising

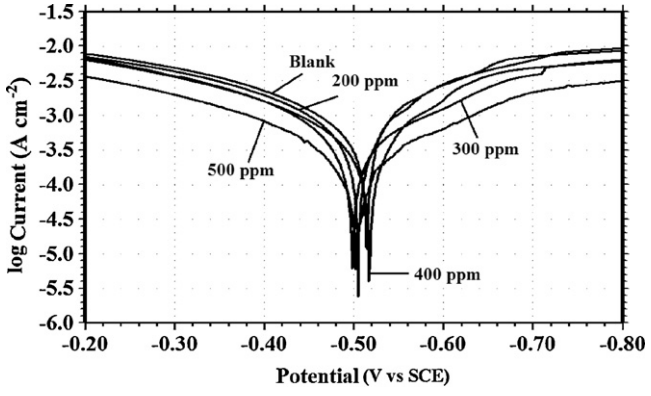

Fig. 1. Tafel polarization curves for cast iron in 1 M HCl (blank) in presence and absence of different concentrations of inhibitor **C** (200–500 ppm) at 298 ± 1 K.

Table 3
Tafel polarization parameter values for the corrosion of cast iron in 1 M HCl both in the presence and absence of inhibitors at 298 ± 1 K.

Inhibitor	Concentration of inhibitor (ppm)	I_{corr} (μA cm^{-2})	E_{corr} (mV *vs* SCE)	b_c (mV/dec)	b_a (mV/dec)	IE%	θ
Blank	0	509	−515	5.25	5.51	–	–
A	200	297	−513	7.18	12.04	42.0	0.42
	300	249	−545	7.72	10.50	51.0	0.51
	400	202	−503	6.10	5.94	60.0	0.60
	500	153	−498	5.95	5.37	69.7	0.70
B	200	178	−539	4.76	5.08	65.0	0.65
	300	162	−497	5.03	4.98	68.1	0.68
	400	134	−504	5.61	5.69	73.6	0.74
	500	100	−492	5.32	5.39	80.3	0.80
C	200	124.7	−505	6.19	5.31	75.5	0.76
	300	94.9	−498	5.73	5.55	81.3	0.81
	400	71.8	−517	8.61	5.65	85.8	0.86
	500	52.6	−503	5.22	5.52	89.6	0.90

Table 4
EIS parameters for the corrosion of cast iron in 1 M HCl in presence and absence of inhibitors at 298 ± 1 K.

Inhibitor	Concentration of inhibitor (ppm)	R_{ct} (Ω cm^2)	C_{dl} (μF cm^{-2})	IE%	θ
(Blank)	0	27.1	401	–	–
A	200	47.8	127	43.3	0.43
	300	53.8	102	49.7	0.50
	400	68.0	56.4	60.2	0.60
	500	84.8	44.1	68.2	0.68
B	200	76.8	47.1	65.0	0.65
	300	84.9	44.1	68.1	0.68
	400	104.9	25.9	74.2	0.74
	500	142.5	15.1	81.0	0.81
C	200	110.9	25.8	75.5	0.76
	300	134.4	15.8	79.8	0.80
	400	194.8	7.80	86.1	0.86
	500	255.6	4.70	89.4	0.89

surface coverage by the inhibitor molecules. The IE% values calculated from weight loss measurements, polarization measurements were more or less close to the values found in EIS measurements. Electrochemical impedance spectroscopy and polarization curves measurements were repeated at least for 5 times and observed that the results were reproducible.

3.4. Analysis of corrosion-inhibition products

The characteristic changes in FT-IR spectra (Fig. 3) of the inhibitors and the scraped samples were discussed below.

(i) The O—H stretching vibrations for inhibitors **A**, **B**, and **C** appeared at 3416 cm^{-1}, 3400 cm^{-1} and 3438 cm^{-1}, where as for Inh_{ads} the bands were shifted to 3361 cm^{-1}, 3330 cm^{-1}, and 3333 cm^{-1}.
(ii) Stretching due to C=O (1652 cm^{-1}) has shifted to lower frequency (1610 cm^{-1}) region in inhibitor **B** adsorbed onto the cast iron surface, which reveals that the C=O group makes coordination type of bond formation with cast iron surface.

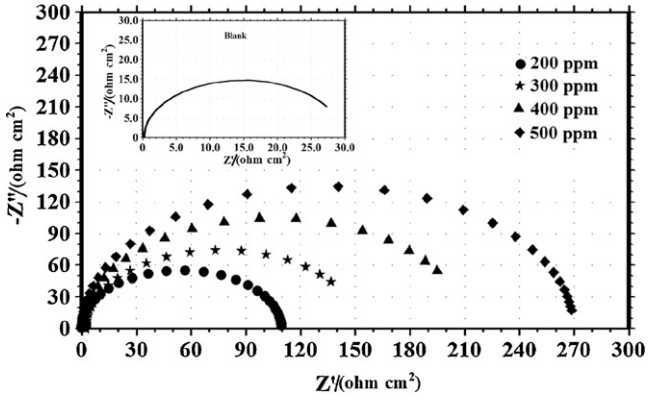

Fig. 2. Nyquist plots of EIS measurements for cast iron in 1 M HCl (blank) in presence and absence of different concentrations of inhibitor **C** at 298 ± 1 K.

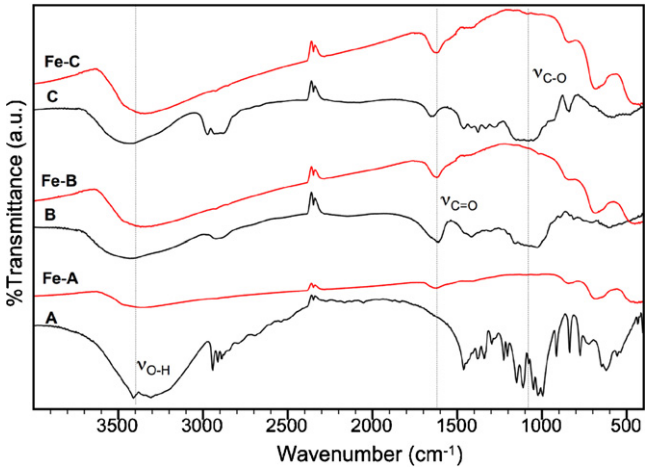

Fig. 3. FT-IR spectrum of inhibitors (**A**, **B**, and **C**) and Inh_{ads} (**Fe-A**, **Fe-B**, and **Fe-C**). Characteristic changes in the ν_{O-H}, $\nu_{C=O}$, and ν_{C-O} of Inh_{ads} indicated the adsorption of inhibitors on the cast iron surface.

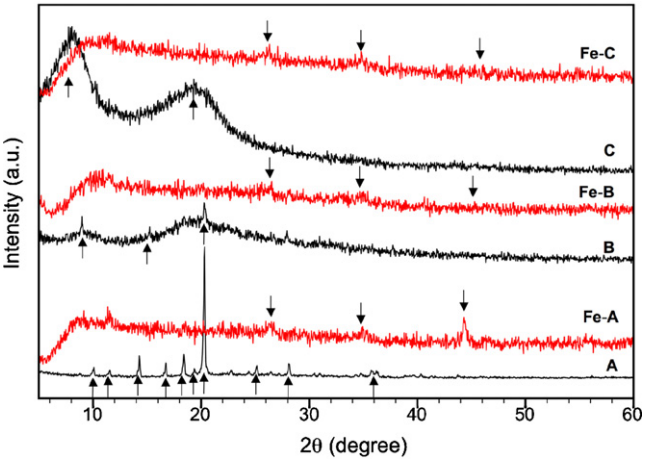

Fig. 4. XRD pattern of inhibitors (**A**, **B**, and **C**) and Inh_{ads} (**Fe-A**, **Fe-B**, and **Fe-C**). The characteristic peaks observed for the inhibitors were shown using 'upward arrow', and development of new peaks in the X-ray diffractogram corresponding to polysaccharide–iron complexes for Inh_{ads} were shown using 'downward arrow'.

(iii) The C—O stretching vibrations present in inhibitors **B** and **C** (1152 and 1161 cm^{-1}) were disappeared in scraped samples as expected.

Though shifts of peaks corresponding to ν_{O-H} and/$\nu_{C=O}$ for the inhibitors were observed, the absence of Fe—O stretching vibration at 425 cm^{-1} (Lobana, Cheema, & Sandhu, 1984) suggests that the mechanism of adsorption at room temperature was most likely to be physisorption.

The X-ray diffractograms of the inhibitors (**A–C**) and Inh_{ads} (**Fe-A**, **Fe-B**, and **Fe-C**) were shown in Fig. 4. Inhibitor **A** exhibited sharp peaks at $2\theta = 10.1–16.6^\circ$, 25.0°, and 28.0° corresponding to the characteristic crystalline phases of glucose. Similarly, inhibitor **B** showed peaks at $2\theta = 8.9^\circ$ and 20.2°, and for **C** characteristic broad peaks at $2\theta = 7.9^\circ$ and 19.4° were observed. The Inh_{ads} (**Fe-A**, **Fe-B**, and **Fe-C**) did not show any peaks corresponding to the inhibitors. The very weak broad peaks observed for all Inh_{ads} at $2\theta = 26.2^\circ$, 34.9°, and 44.3° were may be due to the presence of polysaccharide-iron complex (Berg, Bowen, Hedges, Bereman & Vance, 1984). The results suggest that the inhibitors were potentially adsorbed on the cast iron surface either through physisorption or chemisorption or both.

The morphologies of cast iron surface were observed under SEM both before and after immersion in 1 M HCl in presence and absence of the inhibitors. Specimen immersed in 1 M HCl exhibited a rough surface due to the vigorous attack by the acid and the scratches that were formed during mechanical polishing (see Fig. S7 in supporting information). The iron specimens that were immersed in 1 M HCl + inhibitor showed a relatively smooth surface which is attributed to the effect of inhibitor in retarding the corrosion rate. This was an added evidence for the adsorption of the inhibitor molecules on the cast iron surface.

4. Conclusion

All investigated carbohydrate inhibitors act as effective cast iron corrosion inhibitor in 1 M HCl solution and the inhibition efficiency follows the order **C** > **B** > **A** at room temperature with little differences in their efficiency values in all methods employed. The inhibitor **C** exhibited higher IE% at 298 K, where as at elevated temperatures inhibitor **B** was found to be efficient due to chemisorption mechanism. The addition of KI showed antagonism toward the IE% at lower concentration of KI and synergism at its higher concentration. Electrochemical measurements showed that the inhibitors influence both the anodic and cathodic process (mixed-type inhibitor). The adsorption of inhibitors on cast iron in 1 M HCl solution obeys Langmuir adsorption isotherm. Thermochemical parameters revealed that the inhibitor molecules were adsorbed on cast iron surface *via* both physisorption and chemisorption mechanism. Based on the results from adsorption isotherm, FT-IR, and WAXD, it is concluded that the inhibitors are adsorbed predominantly *via* physisorption than chemisorption. On the whole, gellan gum and hydroxypropyl cellulose can act as potential inhibitors against the corrosion of cast iron in acidic solutions and they act *via* both physical and chemical interactions.

Appendix A. Supplementary data

Supplementary data associated with this article can be found, in the online version, at http://dx.doi.org/10.1016/j.carbpol.2013.02.069.

References

Abdallah, M. (2004). Guar gum as corrosion inhibitor for carbon steel in sulfuric acid solutions. *Portugaliae Electrochimica Acta*, *22*, 161–175.
Ammar, I., Darwish, S., & Etman, M. (1967). Adsorption of iodide ions on polarized iron. *Electrochimica Acta*, *12*, 485–494.
Ammar, I. A., & Khorafi, F. M. E. (1973). Adsorbability of thiourea on iron cathodes. *Werkstoffe and Korrosion*, *24*, 702–707.
Bayol, E., Gurten, A. A., Dursun, M., & Kayakirilmaz, K. (2008). Adsorption behavior and inhibition corrosion effect of sodium carboxymethyl cellulose on mild steel in acidic medium. *Acta Physico-Chimica Sinica*, *24*, 2236–2243.
Behpour, M., Ghoreishi, S. M., Soltani, N., Niasari, M. S., Hamadanian, M., & Gandomi, A. (2008). Electrochemical and theoretical investigation on the corrosion inhibition of mild steel by thiosalicylaldehyde derivatives in hydrochloric acid solution. *Corrosion Science*, *50*, 2172–2181.
Bello, M., Ochoa, N., Balsamo, V., López-Carrasquero, F., Coll, S., Monsalve, A., & González, G. (2010). Modified cassava starches as corrosion inhibitors of carbon steel: An electrochemical and morphological approach. *Carbohydrate Polymers*, *82*, 561–568.
Berg, K. A., Bowen, L. H., Hedges, S. W., Bereman, R. D., & Vance, C. T. (1984). Identification of ferrihydrite in polysaccharide iron complex by Mossbauer spectroscopy and X-ray diffraction. *Journal of Inorganic Biochemistry*, *22*, 125–135.
Gopiraman, M., Selvakumaran, N., Kesavan, D., & Karvembu, R. (2012). Adsorption and corrosion inhibition behaviour of N-(phenylcarbamothioyl) benzamide on mild steel in acidic medium. *Progress in Organic Coatings*, *73*, 104–111.
Huheey, J. E., Keiter, E. A., Keiter, R. L., & Medhi, O. K. (1993). Chapter 14, coordination chemistry: Bonding. In *Inorganic chemistry: Principles of structure and reactivity* (4th ed.). USA: Pearson Education Inc., p. 439
Kesavan, D., Gopiraman, M., & Sulochana, N. (2012). Green inhibitors for corrosion of metals: A review. *Chemical Science Review and Letters*, *1*, 1–8.
Kesavan, D., Muthu Tamizh, M., Gopiraman, M., Sulochana, N., & Karvembu, R. (2012). Physicochemical studies of 4-substituted N-(2-mercaptophenyl)-salicylideneimines: Corrosion inhibition of mild steel in an acid medium. *Journal of Surfactants and Detergents*, *15*, 567–576.
Klemm, D., Schmauder, H. P., & Heinze, T. (2002). E. J. Vandamme, S. D. Baets, & A. Steinbuchel (Eds.), *Biopolymers, polysaccharides II: Polysaccharides from eukaryotes* (pp. 2–3). CA, USA: Wiley-VCH.
Lagrenee, M., Mernari, B., Bouanis, M., Traisnel, M., & Bentiss, F. (2002). Study of the mechanism and inhibiting efficiency of 3,5-bis(4-methylthiophenyl)-4H-1, 2,4-triazole on mild steel corrosion in acidic media. *Corrosion Science*, *44*, 573–588.
Li, X., Deng, S., Mu, G., Fu, H., & Yang, F. (2008). Inhibition effect of nonionic surfactant on the corrosion of cold rolled steel in hydrochloric acid. *Corrosion Science*, *50*, 420–430.
Lobana, T. S., Chemma, H. S., & Sandhu, S. S. (1984). X-ray diffraction (powder), E.S.R. and other spectral studies of tris[methylenebis(diphenylphosphine oxide)]iron(III) perchlorate. *Transition Metal Chemistry*, *9*, 330–331.
Mobin, M., Khan, M. A., & Parveen, M. (2011). Inhibition of mild steel corrosion in acidic medium using starch and surfactants additives. *Journal of Applied Polymer Science*, *121*, 1558–1565.
Noor, E. A. (2007). Temperature effects on the corrosion inhibition of mild steel in acidic solutions by aqueous extract of fenugreek leaves. *International Journal of Electrochemical Science*, *2*, 996–1017.
Rajeswari, V., Kesavan, D., Gopiraman, M., & Viswanathamurthi, P. (2013). Inhibition of cast iron corrosion in acid, base, and neutral media using Schiff base derivatives. *Journal of Surfactants and Detergents*, http://dx.doi.org/10.1007/s11743-013-1439-3 (published online)
Solomon, M. M., Umoren, S. A., Udosoro, I. I., & Udoh, A. P. (2010). Inhibitive and adsorption behaviour of carboxymethyl cellulose on mild steel corrosion in sulphuric acid solution. *Corrosion Science*, *52*, 1317–1325.
Umoren, S. A., Obotl, I. B., Ebenso, E. E., & Okafor, P. C. (2008). Eco-friendly inhibitors from naturally occurring exudate gums for aluminium corrosion inhibition in acidic medium. *Portugaliae Electrochimica Acta*, *26*, 267–282.

Umoren, S. A., Ogbobe, O., Igwe, I. O., & Ebenso, E. E. (2008). Inhibition of mild steel corrosion in acidic medium using synthetic and naturally occurring polymers and synergistic halide additives. *Corrosion Science*, *50*, 1998–2006.
Umoren, S. A., Solomon, M. M., Udosoro, I. I., & Udoh, A. P. (2010). Synergistic and antagonistic effects between halide ions and carboxymethyl cellulose for the corrosion inhibition of mild steel in sulphuric acid solution. *Cellulose*, *17*, 635–648.
Yang, C.-H. (1998). Statistical mechanical study on the Freundlich isotherm equation. *Journal of Colloid and Interface Science*, *208*, 379–387.